doi:10.1093/brain/awy187 BRAIN 2018: 141; 2631–2643 | 2631

BRAIN
A JOURNAL OF NEUROLOGY

High-frequency stimulation of anterior nucleus of thalamus desynchronizes epileptic network in humans

Tao Yu,[1] Xueyuan Wang,[1] Yongjie Li,[1] Guojun Zhang,[1] Gregory Worrell,[2] Patrick Chauvel,[3] Duanyu Ni,[1] Liang Qiao,[1] Chang Liu,[1] Liping Li,[4] Liankun Ren[4] and Yuping Wang[4]

Epilepsy has been classically seen as a brain disorder resulting from abnormally enhanced neuronal excitability and synchronization. Although it has been described since antiquity, there are still significant challenges achieving the therapeutic goal of seizure freedom. Deep brain stimulation of the anterior nucleus of the thalamus has emerged as a promising therapy for focal drug-resistant epilepsy; the basic mechanism of action, however, remains unclear. Here, we show that desynchronization is a potential mechanism of deep brain stimulation of the anterior nucleus of the thalamus by studying local field potentials recordings from the cortex during high-frequency stimulation (130 Hz) of the anterior nucleus of the thalamus in nine patients with drug-resistant focal epilepsy. We demonstrate that high-frequency stimulation applied to the anterior nucleus of the thalamus desynchronizes ipsilateral hippocampal background electrical activity over a broad frequency range, and reduces pathological epileptic discharges including interictal spikes and high-frequency oscillations. Furthermore, high-frequency stimulation of the anterior nucleus of the thalamus is capable of decoupling large-scale neural activity involving the hippocampus and distributed cortical areas. We found that stimulation frequencies ranging from 15 to 45 Hz were associated with synchronization of hippocampal local field potentials, whereas higher frequencies (>45 Hz) promoted desynchronization of ipsilateral hippocampal activity. Moreover, reciprocal effective connectivity between the anterior nucleus of the thalamus and the hippocampus was demonstrated by hippocampal-thalamic evoked potentials and thalamic-hippocampal evoked potentials. In summary, high-frequency stimulation of the anterior nucleus of the thalamus is shown to desynchronize focal and large-scale epileptic networks, and here is proposed as the mechanism for reducing seizure generation and propagation. Our data also demonstrate position-specific correlation between deep brain stimulation applied to the anterior nucleus of the thalamus and patients with temporal lobe epilepsy and seizure onset zone within the Papaz circuit or limbic system. Our observation may prove useful for guiding electrode implantation to increase clinical efficacy.

1 Beijing Institute of Functional Neurosurgery, Xuanwu Hospital, Capital Medical University, 100053, Beijing, China
2 Mayo Systems Electrophysiology Laboratory, Departments of Neurology and Physiology and Biomedical Engineering, Mayo Clinic, Rochester, MN 55905, USA
3 UMR 1106 INSERM, Institut de Neurosciences des Systemes, Aix-Marseille University, Marseille, France; Epilepsy Center, Cleveland Clinic, Cleveland, OH 44195, USA
4 Comprehensive Epilepsy Center of Beijing, The Beijing Key Laboratory of Neuromodulation, Department of Neurology, Xuanwu Hospital, Capital Medical University, 100053, Beijing, China

Correspondence to: Liankun Ren
Department of Neurology, Xuanwu Hospital, Capital Medical University, 45 Changchun Street, 100053, Beijing, China
E-mail: rlkbrain2000@yahoo.com

Correspondence may also be addressed to: Yuping Wang
E-mail: wangyuping01@sina.cn

Received October 13, 2017. Revised May 23, 2018. Accepted May 26, 2018. Advance Access publication July 6, 2018

Keywords: epilepsy; anterior nucleus of thalamus; high frequency stimulation; desynchronization; stereoelectroencephalography

Abbreviations: ANT = anterior nucleus of thalamus; DBS = deep brain stimulation; SEEG = stereoelectroencephalography

Introduction

Epilepsy is a common neurological condition affecting people of all ages worldwide. Although seizures and epilepsy have been described since antiquity (Panteliadis *et al.*, 2017), the therapeutic goal of seizure freedom is not achieved for many patients. The treatment choices for epilepsy currently include multiple modalities (Santulli *et al.*, 2016; Dalkilic, 2017; Golyala and Kwan, 2017). Antiepileptic drugs are the mainstay for treatment, mainly through enhancement of inhibitory neurotransmission, attenuation of excitatory transmission, and modulation of presynaptic neurotransmitter release (Loscher *et al.*, 2013; Vajda and Eadie, 2014). For up to 30% of patients who continue to experience recurrent seizures despite optimal medical therapy, surgical intervention is recognized as a powerful approach to achieve seizure freedom if the epileptogenic focus is delineated precisely and resected completely (Engel, 1996; Rosenow and Luders, 2001; Kwan *et al.*, 2011). Nevertheless, epilepsy surgery remains challenging, and a substantial proportion of patients are not candidates for resective surgery for various reasons, including multiple seizure foci, poor localization of the seizure focus, the epileptogenic focus overlaps with the eloquent cortex, or inability to tolerate surgery due to ongoing medical conditions (West *et al.*, 2015; Jette *et al.*, 2016; Jin *et al.*, 2016). Thus, alternative therapeutic strategies are needed for these patients.

Over the last few decades, deep brain stimulation (DBS) has emerged as a viable therapy for drug-resistant epilepsy (Theodore and Fisher, 2004; Fisher and Velasco, 2014). A number of potential brain targets have been investigated. In particular, the anterior nucleus of thalamus (ANT), consisting of the anteroventral, anterodorsal, and anteromedial nuclei, was recognized as a potential target because of its central connectivity and possible role in propagation of seizure activity (Wyckhuys *et al.*, 2009; Child and Benarroch, 2013). Upton and colleagues (1985) first introduced DBS of the ANT followed by several open-label pilot studies (Hodaie *et al.*, 2002; Kerrigan *et al.*, 2004; Andrade *et al.*, 2006; Lim *et al.*, 2007), demonstrating evidence of efficacy and safety in drug-resistant focal epilepsy. Recently, in a large randomized controlled study of ANT stimulation with long-term follow-up (Fisher *et al.*, 2010; Salanova *et al.*, 2015), there was a 56% median seizure reduction at the second year and a 69% median seizure reduction at the fifth year in patients with drug-resistant focal epilepsy. This study also showed that patients with temporal lobe epilepsy achieved greater benefit than those with extratemporal lobe or multifocal seizures.

DBS of the ANT has emerged as a promising therapy for focal drug-resistant epilepsy; the exact mechanism of action, however, remains unclear (Udupa and Chen, 2015). The canonical view of epilepsy is that seizures are the result of an imbalance of the excitatory and inhibitory processes. Accordingly, one hypothesis of the mechanism of action of DBS of the ANT is that it normalizes this pathological imbalance in the epileptic network (Tehovnik *et al.*, 2006; Graber and Fisher, 2012; Fisher and Velasco, 2014; Schulze-Bonhage, 2017). For instance, a variety of animal studies argue that the antiepileptic effect of ANT stimulation may be mediated by its effect on adenosine, histamine, and serotonin release (Nishida *et al.*, 2007; Mirski *et al.*, 2009; Miranda *et al.*, 2014). In addition, the application of an electrical field in a hippocampal slice can produce a change in extracellular potassium, a negative direct current shift, a depolarization block of sodium channels, and synaptic inhibition or synaptic depression (Bikson *et al.*, 2001).

A better understanding of the mechanisms underlying DBS of the ANT could have profound implications for refining modulation strategies for seizure control. Hence, we studied the mechanism of neuromodulation in nine patients with refractory focal seizures who underwent stereoelectroencephalography (SEEG) monitoring as part of the evaluation for epilepsy surgery. In these patients, one of the depth electrodes exploring the frontal cortex or the peri-insular cortex was directed towards the thalamus and extended into the ANT after informed consents were obtained. This made it possible to electrically stimulate the ANT and simultaneously record the response in cortex. We demonstrated that high-frequency stimulation of the ANT desynchronizes background local field potentials over a broad frequency band within the ipsilateral hippocampus. Furthermore, both epileptic interictal spikes and high-frequency oscillations within the hippocampus were reduced during the course of high-frequency stimulation of the ANT. Moreover, high-frequency stimulation of the ANT is capable of decoupling large-scale neural activity involving the hippocampus and distributed cortical areas. Thus, we propose desynchronization of local field activity as a potential mechanism of the antiepileptic influence of DBS of the ANT on the seizure-onset zone and epileptic networks. Finally, we show a location-specific correlation between DBS of the ANT and patients with mesial temporal lobe epilepsy based on the distinct mechanism of desynchronization.

Materials and methods

Subjects

We studied nine patients (five males, four females, 25 ± 7.5 years of age) with refractory focal seizures at Xuanwu Hospital, Capital Medical University, Beijing, China. Patients with

destructive lesions such as tumour or encephalomalacia were excluded. All the patients required continuous SEEG recording to delineate the epileptogenic zone or map the eloquent cortex precisely because of insufficient information from non-invasive evaluation including detailed history, neurological examination, neuropsychological testing, neuroimaging, and scalp EEG. The clinical profiles of the patients are summarized in Table 1.

This study was approved by the Institutional Review Board Committee in accordance with the ethical standards of the Declaration of Helsinki, and informed consent was obtained from all patients.

Implantation of depth electrodes

The depth electrodes were semi-rigid platinum/iridium with contacts between 8 and 16, and they were 2 mm in length, 0.8 mm in diameter, and 1.5 mm apart. First, the patient's head was fixed in a Cosman–Roberts–Wells stereotactic frame (Radionics Inc.) with cranium pins under local anaesthesia. A high-resolution CT scan (Siemens) was acquired, and image fusion was performed with the preoperative volumetric T_1 MRI sequences (3.0 T, Siemens) using the NeuroGuide system (STEALTH Framelink, Medtronic, Inc.). In addition, magnetic resonance venography and magnetic resonance angiography sequences (3.0 T, Siemens) were also obtained and fused to avoid major vessel injury in the design of electrodes trajectories. The planning of SEEG, including the number of electrodes and the sites of implantation, was scheduled to explore the hypothetical localization of the seizure-onset zone specific to each patient based exclusively on clinical grounds. For research purposes and after informed consent, one of clinical depth electrodes exploring the frontal cortex or the peri-insular cortex was extended into the ANT after a subtle angle adjustment. Technically, all the depth electrode trajectories were carefully adjusted to avoid the basal ganglia and the thalamostriate veins during the presurgical planning (Supplementary Fig. 1). Under general anaesthesia, the electrodes were inserted one by one using an oblique approach.

Finally, the patient underwent a CT scan after electrode implantation to verify the exact location of each electrode and to check for postoperative complications.

Reconstruction of depth electrodes into the brain

The protocol of reconstruction and localization of the depth electrodes in the brain was described previously (Qin *et al.*,

Table 1 Clinical profiles and implantation of depth electrodes of patients

Patient ID	Age	Sex	Trajectories of depth electrodes	Electrodes/ total contracts	Seizure onset zone	Location of contacts on thalamus
1	19	F	L-HG→Amy; L-TPO→pHippo; L-sFL →aIns; L-iFL→mIns→ANT; L-mFL →BTA	5/80	L-Hippo	ANT, VAmc, VApc
2	32	F	L-TPO→aHippo; L-mTG→BTA; L-iFL →mIns→ANT; L-mFL→Orb; L-mFL →ACC	5/80	L-Hippo	MD, ANT, VApc, RTN
3	24	M	L-mFL→mIns; L-iFL→mIns→ANT; L-sTG→Amy; L-TPO→Hippo; R-TPO→Hippo; R-mFL→mIns	6/96	L-Hippo	MD, ANT, VApc, RTN
4	31	M	L-mFL→ACC; L-iFL→mIns→ANT; L-post-Central→PCC; L-pre-Central →pIns; L-mTG→Hippo; R-iFL→mIns; R-sFL→aIns→Fusi	7/112	L-Hippo	MD, ANT, VAmc, VApc
5	24	M	R-AG→Hippo; R-AG→Fusi; R-mFL →ANT; R-pre-Central→Orb; R-Suprama→pIns; R-TPO→iTG; R-iFL→Orb	7/112	R-Hippo	MD, ANT, VApc, RTN
6	38	F	R-sFL→ACC; R-mFL→ACC; R-iFL→ Orb; R-mFL→mIns; R-iFL→mIns →ANT; R-iTG→TP; R-lOcc→ Hippo	7/112	R-Hippo	ANT, ANT, VApc, RTN
7	13	F	L-post-Central→SMA; L-pre-Central→sFL; L-mFL→sFL; L-iFL→aIns→ANT	4/64	L-superior frontal sulcus	ANT, ANT, VApc, RTN
8	23	M	R-iFL→mIns→ANT; R-sFL→aIns; R-mFL→FP; R-mFL→ACC; R-mFL→Orb	5/80	R-anterior dorsal lateral frontal lobe	MD, ANT, VApc, RTN
9	21	M	L-mFL→mIns; L-iFL→mIns; L-sFL→ ACC; L-AG→PCC; L-AG→pIns; L-AG→Fusi	6/96	L-posterior temporal cortex	MD, ANT, VApc, RTN

ACC = anterior cingulate cortex; AG = angular gyrus; Amy = amygdala; BTA = basal temporal area; pre-Central = precentral gyrus; post-Central = postcentral gyrus; F = female; Fusi = fusiform; iFL = inferior frontal lobe; mFL = mesial frontal lobe; sFL = superior frontal lobe; Hippo = hippocampus; aHippo = anterior hippocampus; pHippo = posterior hippocampus; HG = Heschl's gyrus; aIns = anterior insular; mIns = mesial insular; pIns = posterior insular; L = left; M = male; MD = mediodorsal nucleus; Orb = orbital; lOcc = lateral occipital cortex; PCC = posterior cingulate cortex; R = right; RNT = reticular thalamic nucleus; SMA = supplementary motor area; TP = temporal pole; iTG = inferior temporal gyrus; mTG = mesial temporal gyrus; sTG = superior temporal gyrus; TPO = tempo-parieto-occipital junction; VAmc = ventral anterior nucleus, magnocellular division; VApc = ventral anterior nucleus, parvocellular division.

2017). In brief, cortical surfaces were first reconstructed based on the pre-implant MRI using FreeSurfer image analysis suite (http://surfer.nmr.mgh.harvard.edu) for each patient. The resulting output was a set of coordinates comprising the triangulated pial surface of the subject. The volume T_1 image was also converted into FreeSurfer's conformed space. To determine the location of the depth electrodes, the post-surgery CT was then co-registered to the T_1 image of FreeSurfer's conformed space for each patient. The depth electrodes were readily detected using clustering-based segmentation with optional threshold. After all electrode clusters were chosen correctly, each electrode was stretched out in one direction, and the inside-most point was defined as the starting or deepest point of the electrode trajectory. A centroid estimation step was then applied to the starting point to get a more precise approximation of the optimized electrode contacts. Each electrode track was fitted to a curve. The fitted trajectory of each electrode was represented as a group of equally spaced dots. All the contacts were colour coded and represented in the transparent surface view.

Creation of a 3D atlas of the thalamus

A 3D atlas of the thalamus was created based on the Morel atlas using a similar method as described by Garcia-Garcia *et al.* (2016). Briefly, a colour table for different subcortical structures was created. Each structure was assigned a different number and RGB colour value in this file. Next, the print coronal slice was aligned to the corresponding position in the right-anterior-superior coordinate system, the print coronal slice was set to be half transparent, and the function of mouse penetration was enabled. Every structure in the atlas can be delineated at a voxel resolution of $0.25 \times 0.25 \times 0.25$ mm^3. Manual interpolation was further done in the other two orthogonal axes, avoiding encroachment on adjacent structures. The precise positions of electrode contacts within the thalamus were depicted with the 3D Morel thalamus atlas.

SEEG recording and high-frequency stimulation

Clinically, SEEG was recorded for 7 to 10 days under video monitoring to capture at least three habitual seizures. Signals were recorded by the Micromed EEG data acquisition system with a sampling frequency of 1024 Hz, referencing to a common contact placed subcutaneously.

High-frequency stimulation was delivered extraoperatively by an external stimulator (Model 3628 screener, Medtronic, Inc.). In all the patients, intermittent high-frequency stimulation of 130 Hz, 90-μs pulse width, and intensity of 2 mA was performed with 60- or 90-s on and a 600-s off cycle 5 days after surgery. The stimulus intensity of 2 mA was chosen, similar to clinical stimulation parameters employed clinically (Fisher *et al.*, 2010; Fisher and Velasco, 2014). The stimulation was delivered between pairing neighbouring contacts, with the most medial contact as the cathode, in the thalamus in an effort to stimulate distinct subnuclei of the thalamus. We recorded SEEG from all but stimulated contacts during the high-frequency stimulation. In addition, to clarify the modulated effects of stimulus frequencies, electrical stimulation of the ANT with stepwise increment frequency was applied. The paired contacts on the ANT were selected to be stimulated, and local field potentials on the contacts in seizure onset zone were recorded simultaneously. Stimulation of the ANT began with 5 Hz and increased by 5 Hz in stepwise increments until reaching 130 Hz, lasting 90 s with a time interval of 60 s with a 90-μs pulse width and an intensity of 2 mA.

Cortico-cortical evoked potentials

Cortico-cortical evoked potentials were introduced in recent years to track the cortico-cortical connections *in vivo* in humans (Matsumoto *et al.*, 2004, 2017). The test was also performed extraoperatively during the resting state. In the present study, the hippocampus and ANT were stimulated through two adjacent contacts. The electrical stimulus consisted of a constant current square wave pulse of 0.3 ms duration, a pulse frequency of 1 Hz, with alternating polarity and current intensity of 2 mA. Sixty stimuli were delivered in each session. Electrical pulses were generated with Grass S88 (SUI-7, Astro-Med Inc.). We studied the ipsilateral hippocampo-thalamic and thalamic-hippocampal evoked potentials by stimulating in hippocampus or thalamus to probe the direct connectivity between the hippocampus and ipsilateral ANT.

Data processing and statistical analysis

Local field potentials were recorded on a 128-channel Micromed recording system, sampled at 1024 Hz. All data processing was performed using customized MATLAB codes (MathWorks Inc., Natick, MA) unless stated otherwise. We analysed SEEG data using bipolar referencing to reduce volume conduction and confounding interactions between adjacent contacts.

The spectrograms of local field potentials were analysed using the Chronux software package (www.chronux.org) and were displayed using a logarithmic *z*-axis with colour representing relative intensity. Three bands including 1–30 Hz (conventional band), 30–100 Hz (gamma), and 100–250 Hz (ripple) were used to compare the power changes due to high-frequency stimulation of the ANT. The bipolar montage was used for SEEG, which eliminated most of the 50 Hz line noise and a notch filter was not needed for analysis. Butterworth bandpasses (zero-phase shift) were used to filter local field potentials.

A previously-described automated detection approach was used to identify and then manually verify interictal spikes and high-frequency oscillations (Ren *et al.*, 2015). In brief, for interictal spike detection, raw signals were filtered at 14–70 Hz with a threshold for a significant spike where the filtered envelope was more than three times above the baseline. Because 1024 Hz frequency sampling was used, only ripples (100–250 Hz) in the range of high-frequency oscillations were investigated in the current study. For detecting ripples, raw signals were filtered in the ripple band (Butterworth filter). A threshold for significant ripple oscillations was set at 3 standard deviations (SD) above the mean baseline with at least four consecutive peaks. Notably, because sharp transients can produce oscillations after high-frequency filtering that could be detected as ripples (i.e. Gibbs phenomenon), all detections were visually inspected for

accuracy for each recording session. Occurrence rates of the aforementioned events were calculated.

The construction of the network and analysis were used to evaluate the impact of large-scale connectivity among cortical areas due to high-frequency stimulation of the ANT. For each patient, representative contacts on distinct cortical areas were chosen as nodes in a graph and the strength of correlations of local field potentials between nodes were considered as edges. Local field potentials were processed with band-pass filtered from 0.5 to 30 Hz. This frequency range is thought to play an important role in long-range propagation (Buzsaki and Watson, 2012; Perucca *et al.*, 2014; Martinet *et al.*, 2017). Other frequency bands (0.5–60 Hz, 0.5–100 Hz, and 0.5–200 Hz) were tested, and showed similar results (Supplementary Fig. 2). For each stimulation on or off state, we divided the selected local field potentials into consecutive 1-s epochs (50% overlap). For constructing functional networks from time series data, we used the cross-correlation, which has been consistently validated in the network analysis of seizure (Kramer *et al.*, 2010, 2011; Chu *et al.*, 2012). Significant coupling between two nodes was represented as 1 in the binary network. Otherwise, insignificant coupling was set to zero. The binary networks generated from each window were then averaged across time to create weighted functional networks representative of each DBS on or off state. We preferred to measure network density because it gives a first indication of how well connected a network is during different states (Kramer *et al.*, 2010). The individualized connectivity matrix and network density of the stimulation off and on periods were estimated and compared when stimulation was applied to distinct subnuclei.

The spectral coherence is used to examine the relation between signals. In the present study, the application of coherence was used to study the ANT stimulation frequency-dependent effects on the ipsilateral hippocampal activity. The contact on the thalamus to neighbouring paired stimulated contacts always showed clear artefacts of stimulus frequency, which were used to estimate magnitude-squared coherence with local field potentials on the ipsilateral hippocampus using the Welch method. For each stimulus frequency, average coherence was attained.

Cortico-cortical evoked potentials were averaged time-locked to the onset of each electrical stimulus off-line with a time window of −100 to +500 ms and a low-frequency filter of 1.0 Hz and a high-frequency filter of 250 Hz. Noisy trials containing interictal discharges or artefacts were identified by visual inspection and excluded from further analysis. The main averaged cortico-cortical evoked potentials responses consist of an early sharp response (10–50 ms post-stimulation) and a later slow-wave response (50–250 ms). From stimulus onset up to 10 ms, signals were usually saturated and contaminated with stimulus artefacts; hence, we excluded the first 10 ms from the analysis. These responses have been referred to as N1 and N2, respectively, because the existence of negative voltage deflections during these time periods.

Statistical analysis was performed using customized Matlab code. Differences in power, changes in interictal spikes and ripple occurrence, and large-scale connectivity density between DBS off and on for each paired DBS stimulation were tested using the Wilcoxon rank-sum test method for non-normal distribution data. Time latencies of evoked potentials were compared using two-sample *t*-tests for normal distribution data. A value of $P < 0.05$ was considered to be statistically significant.

Data availability

The data that support this study are available on request. The data are not publicly available as they contain information that could compromise research participant privacy consent.

Results

In total, 52 electrodes were implanted with 832 contacts. There were no surgical-related complications in this group. All the individually reconstructed maps of electrodes into the brain are shown in Fig. 1. Further, the electrodes implanted into the thalamus on the left side were flipped onto the right side and overlaid on a Morel stereotactic atlas of the human thalamus. The precise location of contacts into the subnuclei of the thalamus were detected.

Six patients were finally confirmed with mesial temporal lobe epilepsy, with seizure onset from the unilateral hippocampus. In three other patients, the seizure onset zone was identified as the left superior fontal sulcus, the right anterior dorsal lateral frontal lobe, and the left posterior temporal cortex in Patients 7–9, respectively. Notably, electrodes were successfully implanted into the mediodorsal nucleus, the ANT, and the ventral anterior nucleus of Patients 2–5, 8 and 9. Only the ANT and the ventral anterior nucleus were implanted in Patients 1, 6 and 7. All the patients had at least one electrode implanted into the thalamus that was ipsilateral to the seizure onset zone (Table 1).

High-frequency stimulation of the ANT desynchronizes ipsilateral hippocampal background activity

We analysed the background activity of the ipsilateral seizure onset zone offline during stimulation off and on periods to investigate the changes associated with high-frequency stimulation of different subnuclei of the anterior thalamus.

In all six patients with the seizure onset zone identified in the hippocampus, high-frequency thalamic stimulation produced contact-dependent local field potential changes in ipsilateral hippocampus. In agreement with previous research in animal models (Stypulkowski *et al.*, 2013, 2014; Covolan *et al.*, 2014), we found high-frequency stimulation of the ANT desynchronized broadband local field potentials of the ipsilateral hippocampus, which was characterized by attenuation of ongoing background activity. The changes in local field activity occurred almost instantly with ANT stimulation. The attenuation lasted for the whole on period of stimulation, and the hippocampal background activity quickly recovered to baseline level within seconds after discontinuing the stimulation. Whereas, when high-frequency stimulation was applied to the mediodorsal

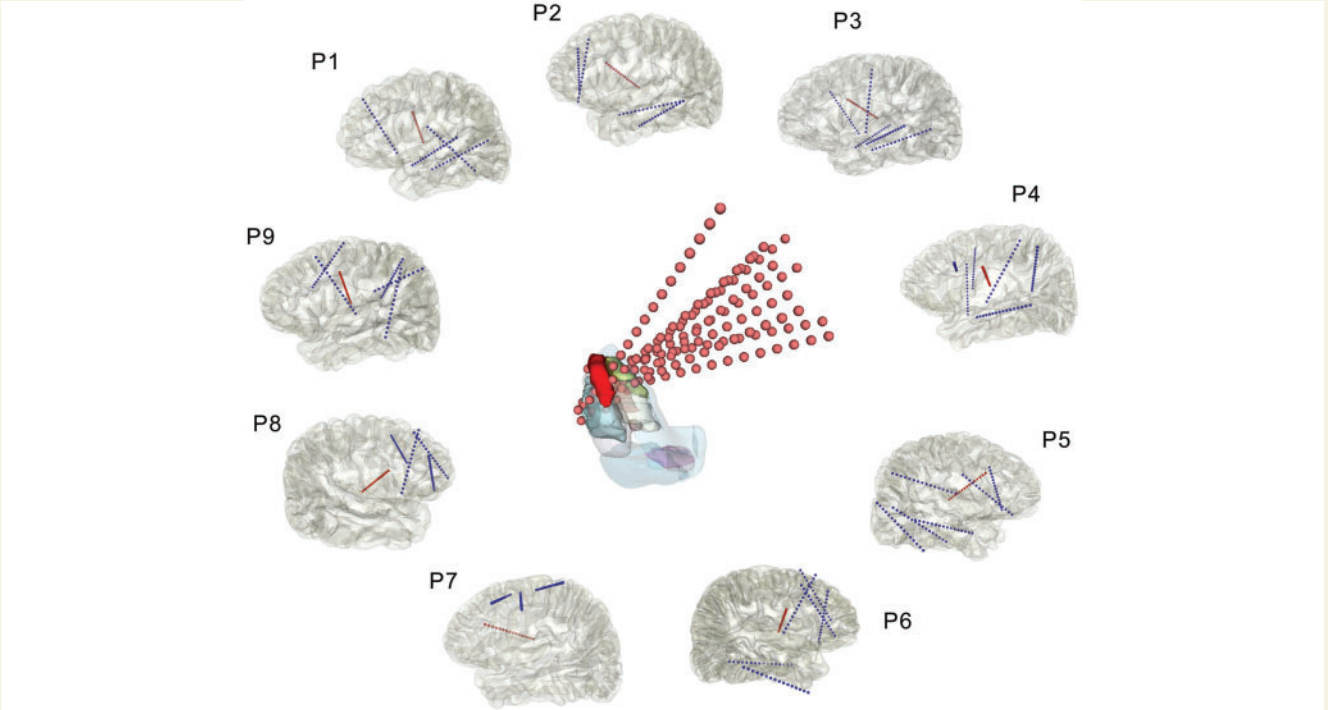

Figure 1 Reconstruction of depth electrodes. The peripheral images show reconstruction of depth electrodes into brain of all nine patients. The red colour-coded electrode was the electrode that was extended into thalamus. The *centre* image showed electrodes into thalamus of all patients overlaid onto the thalamic template (note, the electrodes on left side were flipped into the right side). The blue, red and green colour label the mediodorsal nucleus (MD), anteroventral (AV) of ANT and ventral anterior nucleus (VA), respectively.

nucleus or ventral anterior nucleus of the thalamus, insignificant alterations were observed on the hippocampus (Fig. 2). The effects on other non-epileptogenic cortical areas are shown in Supplementary Fig. 3. The desynchronized effects on hippocampal activity by high-frequency stimulation of the ANT were significantly statistically different from other thalamic subnuclei ($P < 0.05$). In addition, there were no obvious background activity changes of seizure onset zones with high-frequency stimulation of the ANT in three patients with non-mesial temporal lobe epilepsy compared with patients with mesial temporal lobe epilepsy ($P > 0.05$) (see Patient 7 in Supplementary Fig. 4)

High-frequency stimulation of the ANT suppresses hippocampal pathological discharges

The epileptic cortex is characterized by paroxysmal, interictal epileptiform spikes. We investigated whether DBS could suppress pathological epileptiform spikes, which is hypothesized to reflect the ability of high-frequency stimulation to modulate focal epilepsy.

We assessed the changes in the rate of interictal spikes and high-frequency oscillations in the seizure onset zone quantitatively during stimulation on and off cycles. In patients with mesial temporal seizure onset, we observed the location-dependent effects of stimulation on the rates of interictal spikes and high frequency oscillations. Hippocampal interictal spikes and high-frequency oscillation rates were decreased obviously during ANT stimulation on period compared with stimulation of the mediodorsal nucleus and the ventral anterior nucleus across all patients. Figure 3 shows the subnucleus-dependent stimulation effect on epileptic discharges of the hippocampus ($P < 0.05$). By contrast, interictal spikes and high-frequency oscillations rates did not change on contacts sampling the neocortical seizure onset zone in three patients during ANT high-frequency stimulation.

High-frequency stimulations of the ANT disrupted a large-scale epileptic network

In addition to the influence on pathological, epileptiform discharges within the ipsilateral hippocampus we investigated the impact of ANT high-frequency stimulation on large scale epileptic networks.

To compare the functional networks during ANT high frequency stimulation, we evaluated alterations in global connective density. High-frequency stimulation of the ANT decreased the connectivity of the large-scale epileptic network. Interestingly, stimulation of the mediodorsal nucleus and the ventral anterior nucleus also tended to decrease network density (Fig. 4), suggesting indirect or direct connectivity between the thalamus and cortex.

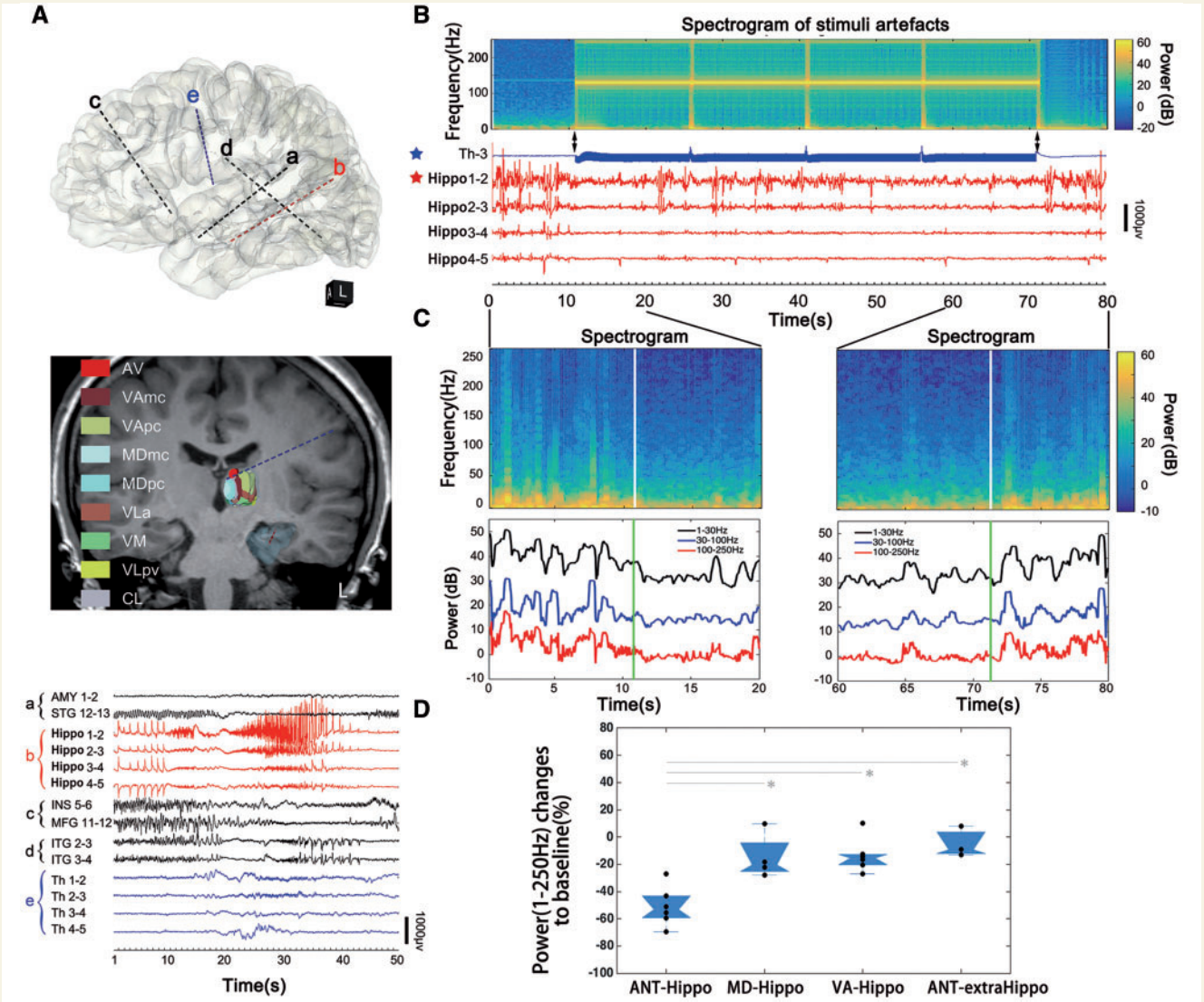

Figure 2 High-frequency stimulation of the ANT desynchronized ispilateral hippocampus background activity. (**A**) *Top*: Reconstruction of depth electrodes into brain (Patient 1). One electrode (blue) was extended into ANT and another electrode (red) was implanted into the ipsilateral hippocampus. *Middle*: Location of the contacts on the thalamic subnuclei, showing contacts 1 and 2 on the ANT. *Bottom*: SEEG epoch showing one focal seizure of impaired awareness arising from the hippocampus (red traces) with low amplitude fast activity, propagating to the ipsilateral thalamus (blue traces) within seconds. (**B**) Stimulus artefacts (black arrows indicate stimulation on and off) on contact 3 of electrode e (blue star) when contacts 1 and 2 were stimulated. The corresponded spectrogram showed stimuli frequency at 130 Hz. The *lower traces* (red) indicated the simultaneous local field potentials (LFPs) on the ipsilateral hippocampus. (**C**) Magnified hippocampal local field potentials (representative trace, hippo1-2, red star), showing the broadband frequency power was reduced with stimulation on and recovered quickly when stimulation off. (**D**) Subnucleus-specific desynchronized effects across patients are displayed with boxplots. MD-hippo = stimulation of mediodorsal nucleus and recorded on the ipsilateral hippocampus, $n = 4$; ANT-Hippo = stimulation of ANT and recorded on the ipsilateral hippocampus, $n = 6$; VA-hippo = stimulation of ventral anterior nucleus and recorded on the ipsilateral hippocampus, $n = 6$; ANT-extrahippo: stimulation of ANT and recorded on the extra-hippocampus seizure onset zone, $n = 3$. Asterisks indicate significance level at $P < 0.05$. AMY = amygdala; AV = anteroventral nucleus; CL = central lateral nucleus; INS = insula; ITG = inferior temporal gyrus; MDmc = mediodorsal nucleus, magnocellular division; MDpc = mediodorsal nucleus, parvocellular division; MFG = medial frontal gyrus; MTLE = mesial temporal lobe epilepsy; STG = superior temporal gyrus; Th = thalamus; VAmc = ventral anterior nucleus, magnocellular division; VApc = ventral anterior nucleus, parvocellular division; VLa = ventral lateral anterior nucleus; VLpv = ventral lateral posterior nucleus, ventral division; VM = ventral medial nucleus.

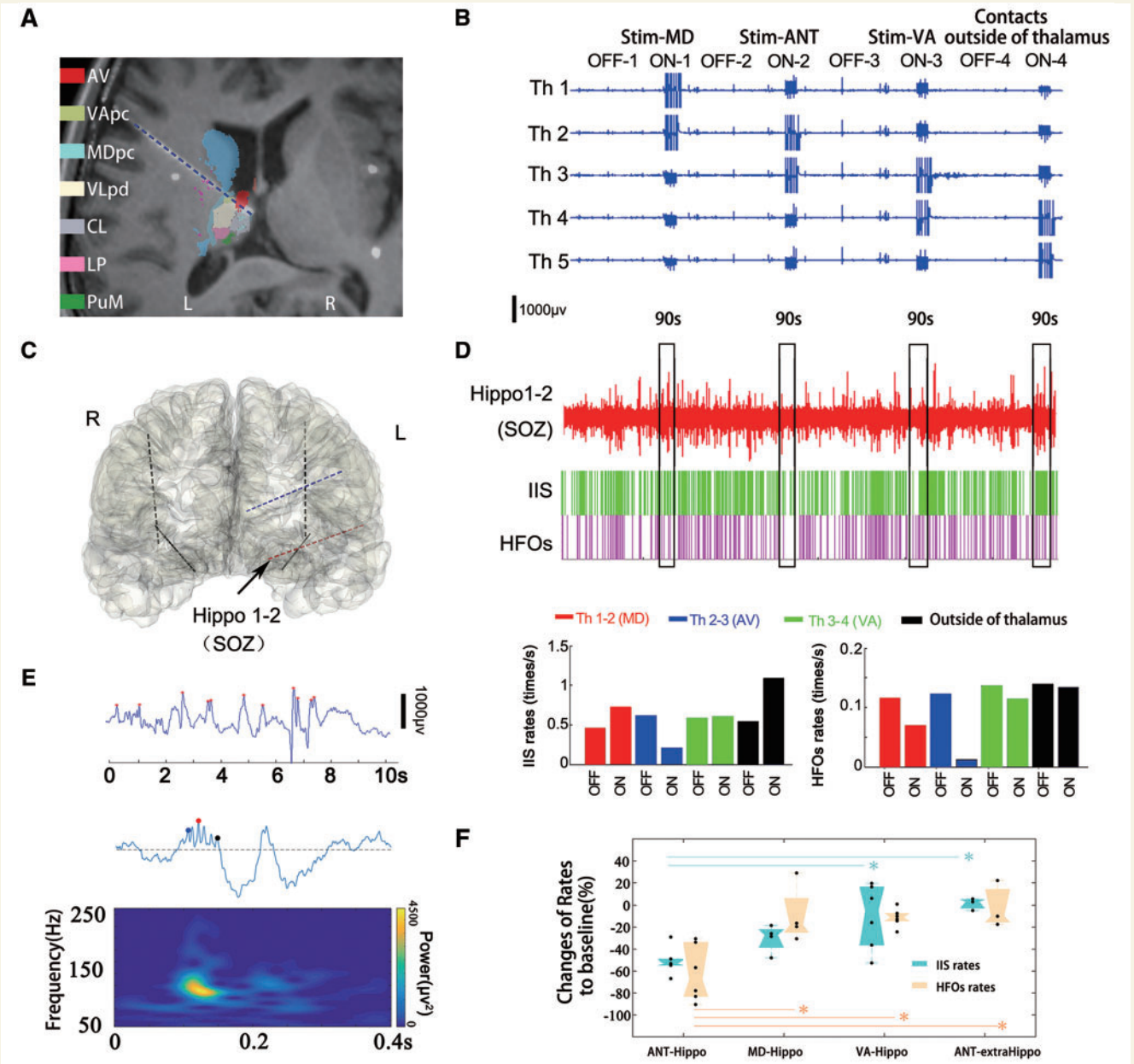

Figure 3 High-frequency stimulation of the ANT suppressed hippocampal pathological discharges in hippocampus.
(**A**) Reconstruction of contacts in the thalamus and depth electrodes into brain. (**B**) The stimulus artefacts on consecutive SEEG epochs showed artefacts of stimulation were delivered in paired contacts serially in thalamus lasting 90 s with a 600-s time interval. (**C**) Patient 3 showing contacts 2 and 3 located on the ANT. One depth electrode was implanted into the ipsilateral hippocampus, which was the seizure onset zone. (**D**) Raster plot of auto-detected interictal spikes and high frequency oscillations on hippocampal trace (Hippo1-2). Interictal spikes and high frequency oscillations decreased obviously when stimulation of ANT (blue bars). (**E**) *Top*: Automatic detected interictal spikes (IIS) with red dot indicating peaks. *Middle*: Automatic detected high frequency oscillations (HFOs) with blue, red and black dot indicating initial, summit and last peak of ripple train, and corresponded spectrogram. (**F**) Suppressed effects on pathological discharges across patients are displayed with boxplots (MD-hippo: $n = 4$; ANT-Hippo: $n = 6$; VA-hippo: $n = 6$; ANT-extrahippo: $n = 3$). Asterisk indicates significance level at $P < 0.05$. PuM = medial pulvinar; SOZ = seizure onset zone; VLpd = ventral lateral posterior nucleus, dorsal division.

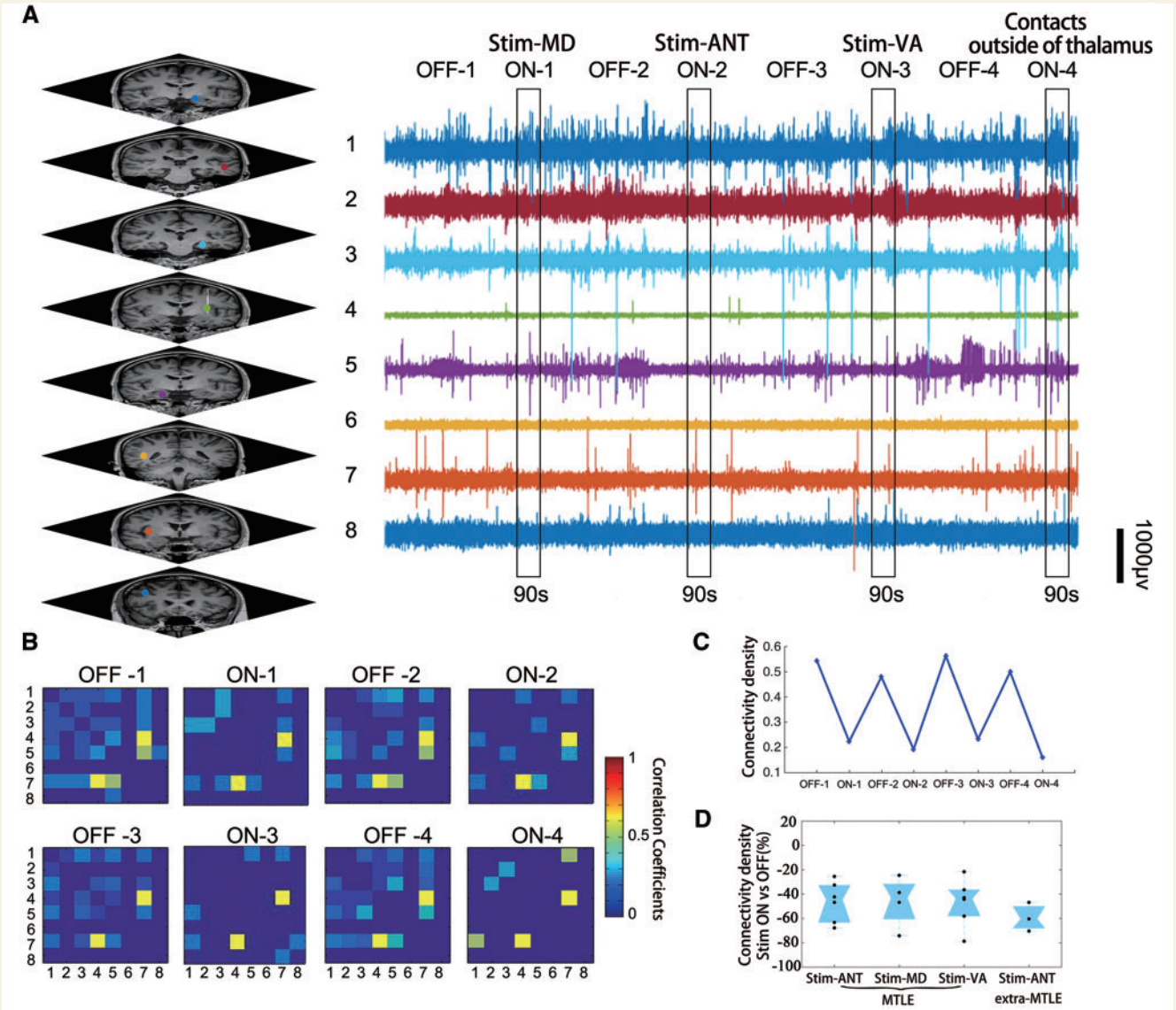

Figure 4 High-frequency stimulation of the ANT interrupted the large-scale cortical network. (**A**) This is the same patient as in Fig. 3. Contacts on distinct cortical structures on MRI (*right*) were colour-coded corresponding to SEEG traces (*left*) during high-frequency stimulation applied to the mediodorsal nucleus (ON-1), ANT (ON-2) and ventral anterior nucleus (ON-3) serially. (**B**) Averaged correlation matrix among distinct cortical areas of each stimulation off and on periods. (**C**) Connectivity density during each stimulation off and on periods, showing that high frequency stimulation reduced the connectivity density no matter which subnucleus was stimulated. (**D**) Decreased connectivity density of the distinct cortical areas due to stimulation applied to the distinct subnucleus in patients with mesial temporal lobe epilepsy (MTLE) (Stim-ANT: $n = 6$; Stim-MD: $n = 4$; Stim-VA: $n = 6$) as well as stimulation of the ANT in three patients with extra-mesial temporal lobe epilepsy ($n = 3$). There are no significant differences of the changes of connectivity density with distinct subnuclei stimulated ($P > 0.05$). MD = mediodorsal nucleus; VA = ventral anterior nucleus.

Stimulation of the ANT produced frequency-dependent synchronization and desynchronization effects

We further examined the frequency-dependent action of ANT electrical stimulation in Patients 4–6. We observed synchronization and increasing spectral coherence activity between the ipsilateral hippocampus and ANT at frequencies from 15 to 45 Hz. By contrast, stimulation frequencies higher than 45 Hz elicited desynchronization in the ipsilateral hippocampus with decreased spectral coherence. Therefore, ANT stimulation produced frequency-dependent synchronization and desynchronization. Electrical stimulation of the ANT at low frequency drives or synchronizes ipsilateral hippocampal activity, whereas stimulation at high frequency (>45 Hz) can desynchronize intrinsic ipsilateral hippocampal activity, as shown in Fig. 5 and Supplementary Fig. 5.

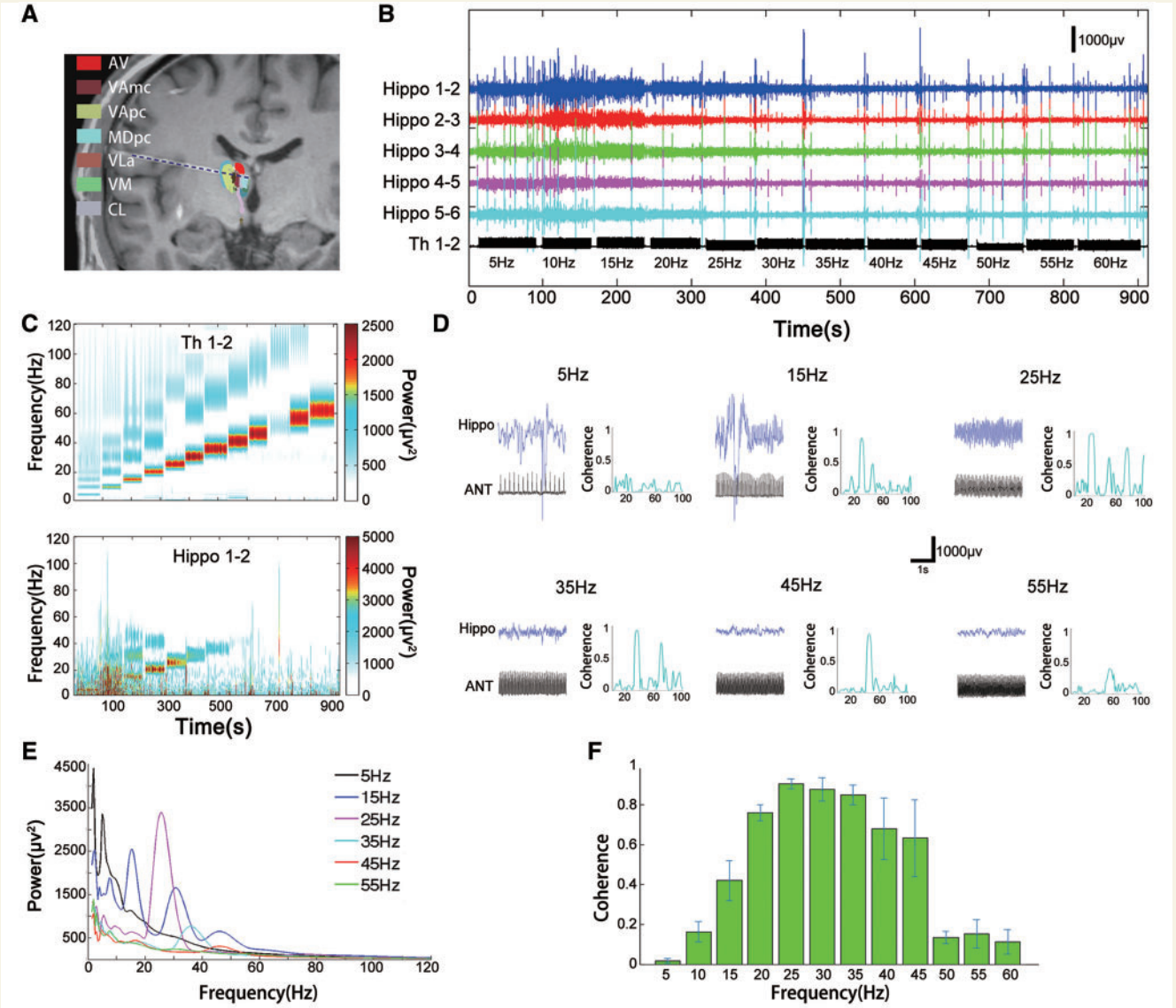

Figure 5 Stimulation frequency-dependent synchronization and desynchronization effects. (**A**) Reconstruction of depth electrodes into the thalamus of Patient 4. (**B**) Stepwise stimulation frequencies of ANT starting from 5 Hz with 5-Hz increment (Th1-2 trace showing stimuli artefacts), and the simultaneous ipsilateral hippocampal local field potentials (LFP) (Hippo1-6). (**C**) Stepwise stimuli artefacts on Th1-2 (*top*) and corresponded local field potentials on representative Hippo1-2 trace (*bottom*) are displayed by time–frequency spectrogram, respectively. Panel **D** shows 3-s epochs of stimuli artefacts on Th1-2 and simultaneous local field potentials on Hippo1-2 at frequencies 5, 15, 25, 35, 45 and 55 Hz, as well as spectral coherence between them. (**E**) Power spectra of local field potentials on Hippo1-2 trace responded to the stimuli on ANT at 5, 15, 25, 35, 45 and 55 Hz. (**F**) Frequency-dependent synchronized and desynchronized effects of the anterior nucleus on ipsilateral hippocampus were consistent with Patients 4–6 (mean ± SD).

The effective connectivity between the hippocampus and the ANT

The effective connectivity between hippocampus and ANT was evaluated using hippocampal-thalamic evoked potentials and thalamic-hippocampal evoked potentials in six patients with mesial temporal seizure onset.

Reciprocal thalamic-hippocampal connectivity was observed in all six patients (Fig. 6). The first negative deflection (N1) component was identified both in hippocampal-thalamic and thalamic-hippocampal evoked potentials with similar time latencies ($P = 0.106$), reflecting direct and bidirectional pathways between the ANT and the ipsilateral hippocampus. The morphology of the N2 component varied between hippocampal-thalamic and thalamic-hippocampal evoked potentials despite the uniformity of N1, suggesting different intrinsic tissue excitatory processes of the thalamus and hippocampus. In addition, responses of other non-epileptogenic cortical areas can be seen in Supplementary Fig. 6.

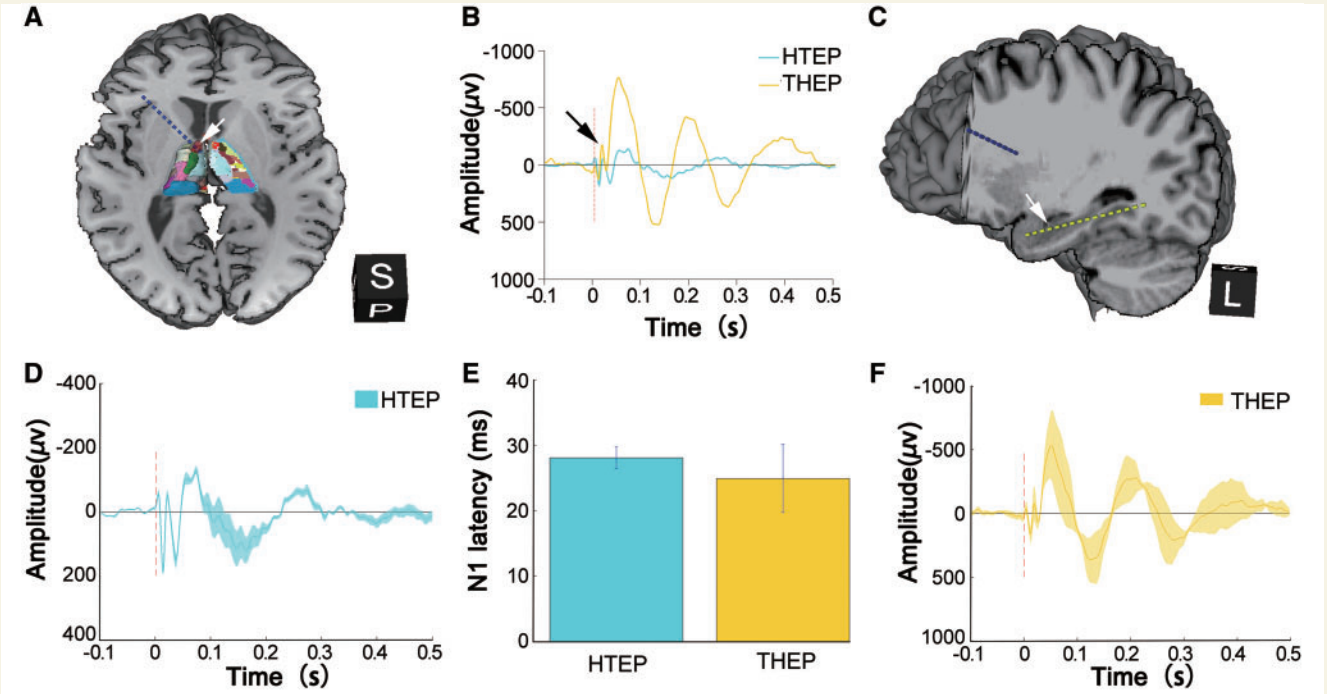

Figure 6 Reciprocal connectivity between hippocampus and the ipsilateral ANT. Reconstruction of the depth electrode on ANT (**A**) and hippocampus (**C**) in Patient 2 (white arrows indicate the recorded and stimulated contacts). (**B**) The early negative potentials (N1, black arrow) were similar between hippocampo-thalamic evoked potentials (HTEP) and thalamic-hippocampal evoked potentials (THEP) regardless of the varied waveform of later potentials. The averaged hippocampo-thalamic (**D**) and thalamic-hippocampal evoked potentials (**F**) of six patients (mean shaded with standard errors). (**E**) There are insignificant difference of the N1 time latencies between hippocampo-thalamic and thalamic-hippocampal evoked potentials (mean ± SD: 28.0 ± 1.7 ms versus 24.9 ± 5.2 ms, $P = 0.106$). Cubes in **A** and **C**: L = left view; P = posterior view; S = superior view.

Discussion

Our findings, based on the investigation of electrical stimulation of the ANT in patients with refractory focal seizures undergoing SEEG monitoring, demonstrate that desynchronization is a potential mechanism of action for the suppression of seizures by DBS of the ANT.

The application of SEEG provides local field potential recordings from deep brain substrates, such as the bottom of the sulcus, hippocampus, amygdala and insula. Previously, few pioneering studies have investigated cortico-thalamic networks in seizures propagation and sleep using SEEG in humans (Guye *et al.*, 2006; Rosenberg *et al.*, 2009; Evangelista *et al.*, 2015; Mak-McCully *et al.*, 2017). In the present study, patients consented for a research study, and SEEG depth electrodes targeting the frontal or peri-insular cortex were extended into ANT. We were extremely cautious during the planning stage and the surgical procedure using the advanced image techniques to reduce potential risk. Finally, no surgically related complications were reported in this group.

Epilepsy has been classically seen as a common brain disorder resulting from abnormally enhanced neuronal excitability and synchronization (Goldensohn and Purpura, 1963; Kooi, 1966). In the epileptic condition, the impact of synchronization at specific spatiotemporal scales has been well documented in the genesis of interictal spike and high-frequency oscillations that are recognized as biomarkers of epileptogenic tissues (Matsumoto and Ajmonemarsan, 1964; Bragin *et al.*, 1999; Worrell *et al.*, 2008; Keller *et al.*, 2010; Zijlmans *et al.*, 2012). In particular, high-frequency oscillations have been recently suggested to play a role in merging neurons of micro-domains into the formation of a seizure (Demont-Guignard *et al.*, 2012). Ictal, a focal seizure can be considered to be a local event beginning in a limited region and sequentially spreading to recruit connected areas through both pathological and normal brain tissue (Kramer *et al.*, 2010; Kramer and Cash, 2012; Burns *et al.*, 2014). Therefore, synchronization between brain regions is crucial to seizure spread.

Desynchronization is known to be associated with resistance to epileptic activity (Medeiros Dde and Moraes, 2014; Stypulkowski *et al.*, 2014; Kim *et al.*, 2017). Our study showed that high-frequency stimulation of the ANT is capable of desynchronizing background activity of the ipsilateral hippocampus, suppressing interictal spikes and ripples of the ipsilateral hippocampus and disrupting the connectivity across cortical areas. Therefore, we hypothesize that the clinical efficacy of DBS of the ANT is attributable to the desynchronization of focal and large-scale epileptic networks, and lowering the network level of excitation. According to this hypothesis, a seizure can be aborted

focally and impeded from propagation by induction of desynchronization. The frequency-dependent modulation effects, as our data further demonstrated, suggest that low-frequency stimulation of the anterior nucleus of the thalamus is prone to provoke seizures, potentially in contrast with high-frequency stimulation (Mirski *et al.*, 1997; Murrow, 2014; Wang *et al.*, 2016), which might be different from the action of low-frequency stimulation of epileptogenic foci directly (Gaito *et al.*, 1980; Yamamoto *et al.*, 2002; Kile *et al.*, 2010).

Therapeutic interventions directed at specific circuitry can selectively affect the particular types of seizures that depend on that circuitry (Fisher *et al.*, 2010; Salanova *et al.*, 2015). Given the anatomy of the circuit of Papaez or limbic system, it is not surprising that the mutual modulatory effect of DBS of the ANT are more significant on the hippocampus than on those of our other explored areas, which is further supported by evoked potentials showing robust reciprocal effective cortico-hippocampal connectivity. Hence, our data suggest that patients with mesial temporal lobe epilepsy might be good candidates for DBS of the ANT. A primary limitation of the current study is the small number of patients, and confirmation will require systematic investigation in a larger number of patients.

Acknowledgements

The authors would like to thank Wei Du, Cuiping Xu, Xiaoxia Zhou, Yuanyuan Piao and Liang Wang for technical assistance. We would like to thank Professor. Robert Fisher for critical comments and revision of the manuscript. The authors are enormously indebted to the patients that participated in this study, as well as the nursing and physician staff at each facility.

Funding

T.Y. was funded by National Natural Science Foundation of China 81771395. L.R. was funded by National Natural Science Foundation of China 81571271. Y.W. was funded by Beijing Municipal Science & Technology Commission Z161100002616001, Beijing Municipal Education Commission TJSH20161002502 and National Natural Science Foundation of China 81771398.

Supplementary material

Supplementary material is available at *Brain* online.

References

Andrade DM, Zumsteg D, Hamani C, Hodaie M, Sarkissian S, Lozano AM, et al. Long-term follow-up of patients with thalamic deep brain stimulation for epilepsy. Neurology 2006; 66: 1571–3.

Bikson M, Lian J, Hahn PJ, Stacey WC, Sciortino C, Durand DM. Suppression of epileptiform activity by high frequency sinusoidal fields in rat hippocampal slices. J Physiol 2001; 531 (Pt 1): 181–91.

Bragin A, Engel J Jr, Wilson CL, Fried I, Buzsaki G. High-frequency oscillations in human brain. Hippocampus 1999; 9: 137–42.

Burns SP, Santaniello S, Yaffe RB, Jouny CC, Crone NE, Bergey GK, et al. Network dynamics of the brain and influence of the epileptic seizure onset zone. Proc Natl Acad Sci USA 2014; 111: E5321–30.

Buzsaki G, Watson BO. Brain rhythms and neural syntax: implications for efficient coding of cognitive content and neuropsychiatric disease. Dialogues Clin Neurosci 2012; 14: 345–67.

Child ND, Benarroch EE. Anterior nucleus of the thalamus: functional organization and clinical implications. Neurology 2013; 81: 1869–76.

Chu CJ, Kramer MA, Pathmanathan J, Bianchi MT, Westover MB, Wizon L, et al. Emergence of stable functional networks in long-term human electroencephalography. J Neurosci 2012; 32: 2703–13.

Covolan L, de Almeida AC, Amorim B, Cavarsan C, Miranda MF, Aarao MC, et al. Effects of anterior thalamic nucleus deep brain stimulation in chronic epileptic rats. PLoS One 2014; 9: e97618.

Dalkilic EB. Neurostimulation devices used in treatment of epilepsy. Curr Treat Options Neurol 2017; 19: 7.

Demont-Guignard S, Benquet P, Gerber U, Biraben A, Martin B, Wendling F. Distinct hyperexcitability mechanisms underlie fast ripples and epileptic spikes. Ann Neurol 2012; 71: 342–52.

Engel J Jr. Surgery for seizures. N Engl J Med 1996; 334: 647–52.

Evangelista E, Benar C, Bonini F, Carron R, Colombet B, Regis J, et al. Does the Thalamo-Cortical Synchrony play a role in seizure termination? Front Neurol 2015; 6: 192.

Fisher R, Salanova V, Witt T, Worth R, Henry T, Gross R, et al. Electrical stimulation of the anterior nucleus of thalamus for treatment of refractory epilepsy. Epilepsia 2010; 51: 899–908.

Fisher RS, Velasco AL. Electrical brain stimulation for epilepsy. Nat Rev Neurol 2014; 10: 261–70.

Gaito J, Nobrega JN, Gaito ST. Interference effect of 3 Hz brain stimulation on kindling behavior induced by 60 Hz stimulation. Epilepsia 1980; 21: 73–84.

Garcia-Garcia D, Guridi J, Toledo JB, Alegre M, Obeso JA, Rodriguez-Oroz MC. Stimulation sites in the subthalamic nucleus and clinical improvement in Parkinson's disease: a new approach for active contact localization. J Neurosurg 2016; 125: 1068–79.

Goldensohn ES, Purpura DP. Intracellular potentials of cortical neurons during focal epileptogenic discharges. Science 1963; 139: 840–2.

Golyala A, Kwan P. Drug development for refractory epilepsy: the past 25 years and beyond. Seizure 2017; 44: 147–56.

Graber KD, Fisher RS. Deep brain stimulation for epilepsy: animal models. In: Noebels JL, Avoli M, Rogawski MA, Olsen RW, Delgado-Escueta AV, editors. Jasper's basic mechanisms of the epilepsies. Bethesda, MD: Oxford University Press; 2012.

Guye M, Regis J, Tamura M, Wendling F, McGonigal A, Chauvel P, et al. The role of corticothalamic coupling in human temporal lobe epilepsy. Brain 2006; 129 (Pt 7): 1917–28.

Hodaie M, Wennberg RA, Dostrovsky JO, Lozano AM. Chronic anterior thalamus stimulation for intractable epilepsy. Epilepsia 2002; 43: 603–8.

Jette N, Sander JW, Keezer MR. Surgical treatment for epilepsy: the potential gap between evidence and practice. Lancet Neurol 2016; 15: 982–94.

Jin P, Wu D, Li X, Ren L, Wang Y. Towards precision medicine in epilepsy surgery. Ann Transl Med 2016; 4: 24.

Keller CJ, Truccolo W, Gale JT, Eskandar E, Thesen T, Carlson C, et al. Heterogeneous neuronal firing patterns during interictal epileptiform discharges in the human cortex. Brain 2010; 133 (Pt 6): 1668–81.

Kerrigan JF, Litt B, Fisher RS, Cranstoun S, French JA, Blum DE, et al. Electrical stimulation of the anterior nucleus of the thalamus

for the treatment of intractable epilepsy. Epilepsia 2004; 45: 346–54.
Kile KB, Tian N, Durand DM. Low frequency stimulation decreases seizure activity in a mutation model of epilepsy. Epilepsia 2010; 51: 1745–53.
Kim HY, Hur YJ, Kim HD, Park KM, Kim SE, Hwang TG. Modification of electrophysiological activity pattern after anterior thalamic deep brain stimulation for intractable epilepsy: report of 3 cases. J Neurosurg 2017; 126: 2028–35.
Kooi KA. Voltage-time characteristics of spikes and other rapid electroencephalographic transients: semantic and morphological considerations. Neurology 1966; 16: 59–66.
Kramer MA, Cash SS. Epilepsy as a disorder of cortical network organization. Neuroscientist 2012; 18: 360–72.
Kramer MA, Eden UT, Kolaczyk ED, Zepeda R, Eskandar EN, Cash SS. Coalescence and fragmentation of cortical networks during focal seizures. J Neurosci 2010; 30: 10076–85.
Kramer MA, Eden UT, Lepage KQ, Kolaczyk ED, Bianchi MT, Cash SS. Emergence of persistent networks in long-term intracranial EEG recordings. J Neurosci 2011; 31: 15757–67.
Kwan P, Schachter SC, Brodie MJ. Drug-resistant epilepsy. N Engl J Med 2011; 365: 919–26.
Lim SN, Lee ST, Tsai YT, Chen IA, Tu PH, Chen JL, et al. Electrical stimulation of the anterior nucleus of the thalamus for intractable epilepsy: a long-term follow-up study. Epilepsia 2007; 48: 342–7.
Loscher W, Klitgaard H, Twyman RE, Schmidt D. New avenues for anti-epileptic drug discovery and development. Nat Rev Drug Discov 2013; 12: 757–76.
Mak-McCully RA, Rolland M, Sargsyan A, Gonzalez C, Magnin M, Chauvel P, et al. Coordination of cortical and thalamic activity during non-REM sleep in humans. Nat Commun 2017; 8: 15499.
Martinet LE, Fiddyment G, Madsen JR, Eskandar EN, Truccolo W, Eden UT, et al. Human seizures couple across spatial scales through travelling wave dynamics. Nat Commun 2017; 8: 14896.
Matsumoto H, Ajmonemarsan C. Cellular mechanisms in experimental epileptic seizures. Science 1964; 144: 193–4.
Matsumoto R, Kunieda T, Nair D. Single pulse electrical stimulation to probe functional and pathological connectivity in epilepsy. Seizure 2017; 44: 27–36.
Matsumoto R, Nair DR, LaPresto E, Najm I, Bingaman W, Shibasaki H, et al. Functional connectivity in the human language system: a cortico-cortical evoked potential study. Brain 2004; 127 (Pt 10): 2316–30.
Medeiros Dde C, Moraes MF. Focus on desynchronization rather than excitability: a new strategy for intraencephalic electrical stimulation. Epilepsy Behav 2014; 38: 32–6.
Miranda MF, Hamani C, de Almeida AC, Amorim BO, Macedo CE, Fernandes MJ, et al. Role of adenosine in the antiepileptic effects of deep brain stimulation. Front Cell Neurosci 2014; 8: 312.
Mirski MA, Rossell LA, Terry JB, Fisher RS. Anticonvulsant effect of anterior thalamic high frequency electrical stimulation in the rat. Epilepsy Res 1997; 28: 89–100.
Mirski MA, Ziai WC, Chiang J, Hinich M, Sherman D. Anticonvulsant serotonergic and deep brain stimulation in anterior thalamus. Seizure 2009; 18: 64–70.
Murrow RW. Penfield's prediction: a mechanism for deep brain stimulation. Front Neurol 2014; 5: 213.
Nishida N, Huang ZL, Mikuni N, Miura Y, Urade Y, Hashimoto N. Deep brain stimulation of the posterior hypothalamus activates the histaminergic system to exert antiepileptic effect in rat pentylenetetrazol model. Exp Neurol 2007; 205: 132–44.
Panteliadis CP, Vassilyadi P, Fehlert J, Hagel C. Historical documents on epilepsy: from antiquity through the 20th century. Brain Dev 2017; 39: 457–63.
Perucca P, Dubeau F, Gotman J. Intracranial electroencephalographic seizure-onset patterns: effect of underlying pathology. Brain 2014; 137 (Pt 1): 183–96.
Qin C, Tan Z, Pan Y, Li Y, Wang L, Ren L, et al. Automatic and precise localization and cortical labeling of subdural and depth intracranial electrodes. Front Neuroinform 2017; 11: 10.
Ren L, Kucewicz MT, Cimbalnik J, Matsumoto JY, Brinkmann BH, Hu W, et al. Gamma oscillations precede interictal epileptiform spikes in the seizure onset zone. Neurology 2015; 84: 602–8.
Rosenberg DS, Mauguiere F, Catenoix H, Faillenot I, Magnin M. Reciprocal thalamocortical connectivity of the medial pulvinar: a depth stimulation and evoked potential study in human brain. Cereb Cortex 2009; 19: 1462–73.
Rosenow F, Luders H. Presurgical evaluation of epilepsy. Brain 2001; 124 (Pt 9): 1683–700.
Salanova V, Witt T, Worth R, Henry TR, Gross RE, Nazzaro JM, et al. Long-term efficacy and safety of thalamic stimulation for drug-resistant partial epilepsy. Neurology 2015; 84: 1017–25.
Santulli L, Coppola A, Balestrini S, Striano S. The challenges of treating epilepsy with 25 antiepileptic drugs. Pharmacol Res 2016; 107: 211–19.
Schulze-Bonhage A. Brain stimulation as a neuromodulatory epilepsy therapy. Seizure 2017; 44: 169–75.
Stypulkowski PH, Stanslaski SR, Denison TJ, Giftakis JE. Chronic evaluation of a clinical system for deep brain stimulation and recording of neural network activity. Stereotact Funct Neurosurg 2013; 91: 220–32.
Stypulkowski PH, Stanslaski SR, Jensen RM, Denison TJ, Giftakis JE. Brain stimulation for epilepsy–local and remote modulation of network excitability. Brain Stimul 2014; 7: 350–8.
Tehovnik EJ, Tolias AS, Sultan F, Slocum WM, Logothetis NK. Direct and indirect activation of cortical neurons by electrical microstimulation. J Neurophysiol 2006; 96: 512–21.
Theodore WH, Fisher RS. Brain stimulation for epilepsy. Lancet Neurol 2004; 3: 111–18.
Udupa K, Chen R. The mechanisms of action of deep brain stimulation and ideas for the future development. Prog Neurobiol 2015; 133: 27–49.
Upton AR, Cooper IS, Springman M, Amin I. Suppression of seizures and psychosis of limbic system origin by chronic stimulation of anterior nucleus of the thalamus. Int J Neurol 1985; 19–20: 223–30.
Vajda FJ, Eadie MJ. The clinical pharmacology of traditional antiepileptic drugs. Epileptic Disord 2014; 16: 395–408.
Wang Y, Liang J, Xu C, Wang Y, Kuang Y, Xu Z, et al. Low-frequency stimulation in anterior nucleus of thalamus alleviates kainate-induced chronic epilepsy and modulates the hippocampal EEG rhythm. Exp Neurol 2016; 276: 22–30.
West S, Nolan SJ, Cotton J, Gandhi S, Weston J, Sudan A, et al. Surgery for epilepsy. Cochrane Database Syst Rev 2015; (7): CD010541. doi: 10.1002/14651858.CD010541.pub2.
Worrell GA, Gardner AB, Stead SM, Hu S, Goerss S, Cascino GJ, et al. High-frequency oscillations in human temporal lobe: simultaneous microwire and clinical macroelectrode recordings. Brain 2008; 131 (Pt 4): 928–37.
Wyckhuys T, Geerts PJ, Raedt R, Vonck K, Wadman W, Boon P. Deep brain stimulation for epilepsy: knowledge gained from experimental animal models. Acta Neurol Belg 2009; 109: 63–80.
Yamamoto J, Ikeda A, Satow T, Takeshita K, Takayama M, Matsuhashi M, et al. Low-frequency electric cortical stimulation has an inhibitory effect on epileptic focus in mesial temporal lobe epilepsy. Epilepsia 2002; 43: 491–5.
Zijlmans M, Jiruska P, Zelmann R, Leijten FS, Jefferys JG, Gotman J. High-frequency oscillations as a new biomarker in epilepsy. Ann Neurol 2012; 71: 169–78.